The Journal of Adhesion

ISSN: (Print) (Online) Journal homepage: www.tandfonline.com/journals/gadh20

Flexural performance of squared one-sided CFRP patches: modelling and experimental study

Ibrahim Abdelfattah, Francisca Ferreira, Mohamed Nasr Saleh, Paulo NB Reis & Sofia Teixeira De Freitas

To cite this article: Ibrahim Abdelfattah, Francisca Ferreira, Mohamed Nasr Saleh, Paulo NB Reis & Sofia Teixeira De Freitas (2023) Flexural performance of squared one-sided CFRP patches: modelling and experimental study, The Journal of Adhesion, 99:3, 473-491, DOI: 10.1080/00218464.2021.2024807

To link to this article: https://doi.org/10.1080/00218464.2021.2024807

Published online: 16 Jan 2022.

THE JOURNAL OF ADHESION
2023, VOL. 99, NO. 3, 473–491
https://doi.org/10.1080/00218464.2021.2024807

Taylor & Francis
Taylor & Francis Group

Flexural performance of squared one-sided CFRP patches: modelling and experimental study

Ibrahim Abdelfattah[a1], Francisca Ferreira[b1], Mohamed Nasr Saleh[c,d], Paulo NB Reis[e], and Sofia Teixeira De Freitas[c]

[a]Aerospace Structures and Materials Department, University of Science and Technology, Giza, Egypt; [b]Departamento de Ciencias Aeroespaciais, University of Beira Interior, Covilhã, Portugal; [c]Structural Integrity & Composites, Faculty of Aerospace Engineering, Delft University of Technology, Delft, The Netherlands; [d]Advanced Materials Research Centre, Technology Innovation Institute, Masdar City Abu Dhabi, United Arab Emirates; [e]CEMMPRE, Department of Mechanical Engineering, University of Coimbra, Coimbra, Portugal

ABSTRACT

Three-point bending analysis, experimental and numerical, is conducted for three different sizes, 30*30 mm, 40*40 mm and 60*60 mm, of one-sided square cross-ply TEXIPREG HS 160 RM carbon-fiber-reinforced polymer (CFRP) patches as well as intact and notched specimens. The tests are carried out with the aim to study the influence of the patch's size on the flexural properties of the specimen. Hashin-2D damage initiation criterion is adopted to investigate the failure in each ply, and the damage evolution is represented by the stiffness degradation. The intact and notched laminates flexural properties are investigated as well as notch sensitivity. The bonded patch repairs efficiency is investigated in the light of ultimate load, flexural modulus, peel and shear stresses along the bond-line as well as the damage initiation coefficient at critical zones. A significant advancement in the flexural modulus and ultimate load for the repaired laminates is noticed with increasing the patch's size. A Parametric numerical study is conducted to investigate the influence of the patch size on the damage initiation coefficient at the critical zones. The recommended patch's size is 44*44 mm in order to avoid failure initiation at the patch corner overlap on the parent laminate.

ARTICLE HISTORY
Received 18 July 2021
Accepted 27 December 2021

KEYWORDS
Destructive testing; finite element analysis; delamination; epoxy/epoxides; repair

1. Introduction

There are several applications of composite materials in the marine and aerospace industry.[1,2] The choice of composite materials for marine and aerospace structures applications over metals could be justified by their advantages. Composite materials have higher strength to weight ratio, the ability to be fabricated in complex shapes without expensive tooling, and the capability to resist corrosion and fatigue.[2] Composite structures' damage is

CONTACT Sofia Teixeira De Freitas s.teixeiradefreitas@tudelft.nl Structural Integrity & Composites, Faculty of Aerospace Engineering, Delft University of Technology, Delft 2628 CD, The Netherlands

[1]*Contributed-equally*

mostly a combination of matrix and fiber failure in tension and compression as well as delamination. Such damages in composites decrease its structural integrity which leads to short service life. Hence, a repair method for the damaged structure is required to extend its service life. An effective method to repair damaged composites is to apply adhesive bonded patches over the damaged area.[3] One of the important advantages of the bonded patch repair is that there are no new holes introduced to the composite structure during the installation. Hence, no secondary stress concentration is created. In addition, small weight gain, low price and strong design ability of bonded patches give them the privilege over conventional mechanical repair methods.[4] There are several types of bonded joint repairs while the most two common types used in the aerospace industry are scarf joints and external bonded patch repairs.[5] Scarf joints are usually used for long-term repair thanks to their efficiency and absence of interference with the aerodynamic profile of the structure. On the other hand, external bonded patch repairs are faster and simpler so they are mostly used in aircraft to keep them in serviceable condition, temporary, until maintenance.[5] From a geometrical consideration, bonded patch repairs can be achieved by bonding the patch over both sides or single side. However, one of the main challenges of the double-sided patches is the accessibility of the composite structure and the difficulty of following the crack propagation.[6] There are several reasons resulting in the bonded patches' failure such as stress intensity factor in the parent laminate, high increased shear and peel stresses on the adhesive and patch delamination.[4] In external patch repair technique, the damaged area is removed by drilling or cutting a hole, and the parent laminate is repaired by an adhesively bonded patch to increase its strength.[7] However, the performance of adhesively bonded patches is affected by different parameters such as lay-up sequence, thickness, shape of the patch as well as adhesive thickness. It can be noticed from the literature that patch size and stacking sequence play a role in the patch repairs' performance.[8,9] Campilho et al[8] investigated the tensile behavior on repaired laminates with circular patches through experimental and numerical studies. It is reported that the effect of patch size on the patch strength is significant relative to patch thickness effect. Shiuh and Chao[9] conducted a stress analysis study of a damaged composite with a square bonded patch in order to investigate the effect of patch and adhesive parameters on the stress concentration factor reduction. It is concluded that the patch design parameters have more effect on the bonded patches performance than the adhesive parameters. Soutis and Hu[10] investigated the influence of the patch and adhesive thicknesses on the efficiency of external bonded patches based on the reduction of stress concentration. In addition, they conducted experiments on circular and square patches with the same overlap length by applying compressive load, and they concluded that both performed almost the same with a slight increase of 0.35% of compressive strength for the circular patches compared to square patch

strength. On the other hand, Li et al[11] investigated five different shapes of quasi isotropic patches (circle, square, trapezoid, hexagon and lozenge) influence on the static and fatigue tensile strength of adhesively bonded composite repair. Different shapes are found to have dissimilar fatigue strength while the fatigue damage for the adhesive layer is minimal for the square patches. Moreover, the square patches performed the best, in terms of strength, with an increase of 27% in residual strength compared to the unrepaired laminates. Also, it is reported that the ratio of the patch radius relative to the cut-out radius of 2.25 had the highest residual strength for circular patches without investigating the square patches' size influence. Also, Xiao-Jing et al[12] investigated the influence of local concentration on the fatigue and tensile strength of the adhesively bonded patches for quasi isotropic parent laminates, and they reported that square patch repairs have the highest strength through the static tensile tests compared to elliptical, rectangular and circular ones. In addition, they investigated the influence of stacking sequences of circular patches, and it is found that $[45/\text{-}45]_s$ patches have failure strength 25% higher than $[0/90]_s$, but they did not investigate cross-ply parent laminates. Limited work[13] has been performed to investigate the flexural properties and the damage mechanism of external composite patch repairs under bending load. Tsovolos et.al[13] investigated different patch shapes, rectangular and circular, and their influence on the flexural strength of the scarf bonded patch repairs. Nevertheless, there is a need to investigate the influence of square one-sided external patch's size on the repaired specimen integrity. In this study, this is investigated, through three-point bending test with the focus on the patch's size influence on the flexural properties. Three sizes of one-sided square patches are considered here: 30 mm, 40 mm, 60 mm with a stacking sequence of $[0/90]_{2s}$, while a parent laminate stacking sequences is considered $[0/90]_{3s}$. Hence, this research paper aims to extend the investigation of external square bonded patch repairs with the main focus on flexural properties, peel and shear stresses along the bond-line as well as damage initiation on critical zones of the external square one-sided bonded patches.

2. Materials and Manufacturing

The two different laminates were prepared using unidirectional carbon epoxy prepreg, TEXIPREG® Hs 160 REM, provided by the company SEAL, Legnano, Italy, which properties are shown in Table 1. The CFRP laminates were

Table 1. TEXIPREG HS 160 RM lamina properties[14].

Elastic Modulus (GPa)	Poisson's ratio	Shear Modulus (GPa)	Volume fraction
$E_{11} = 109$	$\upsilon_{12} = 0.342$	$G_{12} = 4.315$	0.6
$E_{22} = 8.819$	$\upsilon_{13} = 0.342$	$G_{13} = 4.315$	
$E_{33} = 8.819$	$\upsilon_{23} = 0.380$	$G_{13} = 3.2$	

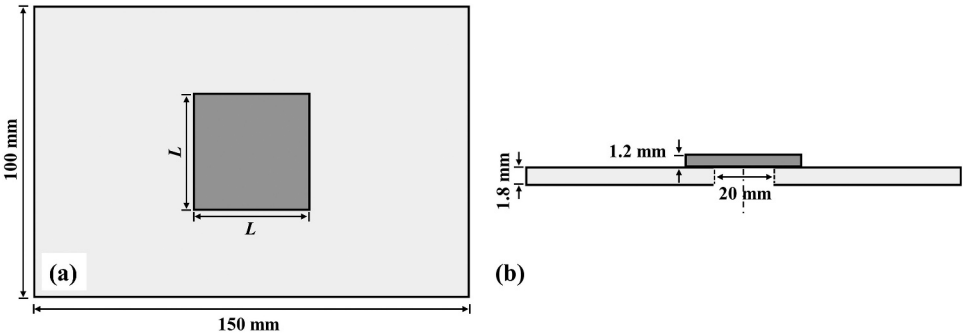

Figure 1. A schematic of the specimen dimensions: a) top view and b) side view.

prepared by prepreg lay-up. For the parent and patch laminates, stacking sequences of $[0/90]_{3s}$ and $[0/90]_{2s}$ were used, respectively. The overall plates were produced using the autoclave process following the manufacturer's recommendations. The parent plates, with a thickness of 1.8 mm, were cut into samples with a single dimension of 150 mm x 100 mm, while the patch laminates, with only 1.2 mm of thickness, were cut into multiple square patch sizes, depending on the chosen dimension of 30, 40 or 60 mm. The cutting was performed using an automated diamond saw machine, in order to achieve the smallest dimension error and clean edges.

For the experimental procedures, the specimens were tested as intact plates, drilled plates (as a representation of the removed damaged area) and the patch repaired plates. For this reason, part of the parent laminates was drilled, creating a centered hole with 20 mm of diameter. For the repaired specimens, the adhesively bonded single patch repair was made using a structural epoxy adhesive 3 M™Scotch-Weld™9323 B/A prepared following the manufacturer's recommendations and mixed with 0.8 g (0.1% by weight) of micro-glass beads (diameter of 150 μm, approximately). The adjacent faces of both the patches as parent plates were roughened using sandpaper (grit size 240) and cleaned in order to increase the adhesion at the adhesive/composite interface. The adhesive was then applied to both sides and the parts were pressed down with weights in order to create a considerable fillet of adhesive around the full thickness of the patch. The thickness of the adhesive was found to be approximately constant and about 0.2 mm. The repaired specimens' geometry is shown in Figure 1.

3. Experimental procedure

The specimens were subjected to three-point bending tests including the intact, notched and patch-repaired ones. The flexural test fixture, shown in Figure 2, was used in order to fix the specimens in the x-, y- and z-axes but allowing the rotation around these directions combined with the vertical

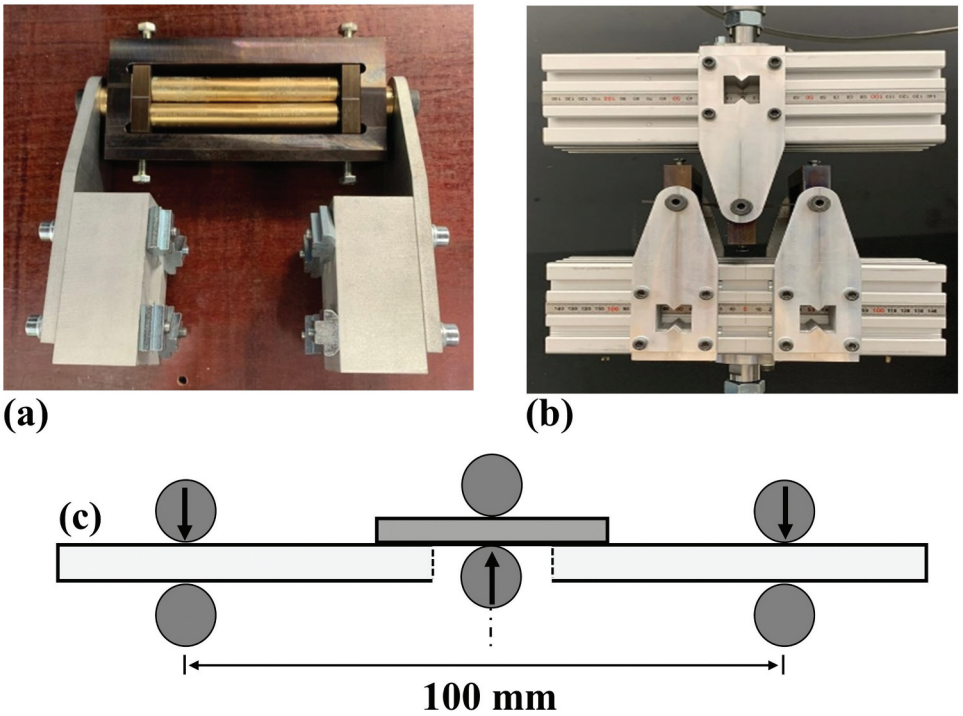

Figure 2. Flexure test setup: a) side view, b) front view and c) schematic of specimen between the rollers.

displacement forced to the central line of the plates. The three-point bending tests were performed using a displacement rate of 3 mm/min with a maximum span of 22 mm and stopped when a clear failure mode was verified or in case of a 60% drop in the load. From these tests the force–displacement curves were obtained and the average load-carrying capacity and bending stiffness calculated.

4. Numerical modelling

The numerical modelling for the 3-point bending test is performed using ABAQUS Standard. Conventional Shell elements were used to model each ply of the composite. In general, elements were set at the size of 2 mm except around the hole where the number of elements employed is increased to capture the stress concentration as shown in Figure 3a. The number of nodes and elements as well as the elements type used for each model are given in Table 2. The two support rollers as well as the loading roller were simulated as rigid cylinders in contact with the composite laminate. The load was applied as an imposed displacement on the reference point on the loading roller while the two support cylinders were rigidly constrained as illustrated in Figure 3b. A parent laminate with a stacking sequence of $[0/90]_{3s}$ with a dimension of

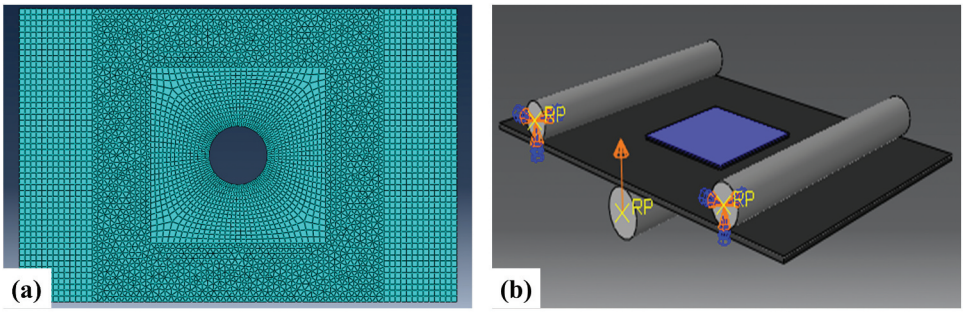

Figure 3. Numerical modelling: a) parent laminate mesh, b) Numerical model boundary conditions.

Table 2. Summary of the FEM model specifications.

Specimen Type	Number of nodes	Number of elements	Element type
Notched	5213	8170	S4R, S3 and R3D4
Intact	4639	4557	S4R and R3D4
Patch-30	9388	12,790	S4R, S3 and R3D4
Patch-40	9643	12,165	S4R, S3 and R3D4
Patch-60	11,323	12,718	S4R, S3 and R3D4

Table 3. TEXIPREG HS 160 RM lamina Strengths for damage initiation[14].

X_{1T} = 1.401 (GPa)	X_{1C} = 1.132 (GPa)	X_{2T} = 0.059 (GPa)
X_{2C} = 0.211 (GPa)	S_{12} = 0.054 (GPa)	S_{13} = 0.1055 (GPa)

Table 4. TEXIPREG HS 160 RM Critical Energy Release rates[16,17].

G_{mc} = 0.9 N/m	G_{mt} = 0.9 N/m
G_{fc} = 143 N/m	G_{ft} = 133 N/m

150 mm *100 mm with a circular cutout of 20 mm diameter was investigated while there were three different square the patch's sizes 30 mm * 30 mm, 40 mm * 40 mm and 60 * 60 mm with the same stacking sequence of $[0/90]_{2s}$.

4.1. Damage model

As no cohesive or adhesive failure was detected in the experiments, the model was simplified to take into account only the damage in the patch and parent laminate. No bond-line damage model was employed. The damage analysis for the parent and patch laminates are investigated using Hashin's 2D damage initiation criterion, and the damage evolution is represented by the stiffness degradation based on each damage mode fracture energy. A viscous regularization scheme is adopted to help overcoming convergence difficulties. For the optimization study, Tsai-Wu damage initiation criterion is adopted since it

gives an indication about the damage initiation coefficient based on the interaction between different stress components using only one parameter, instead of using the four damage variables in Hashin's criterion.[15]

4.2. Hashin's damage initiation

2D Hashin's criterion is implemented for each ply to predict the damage initiation. The four main failure modes are treated separately, and the various failure modes are described throughout the following equations:

Fiber Tension: ($\sigma_{11} \geq 0$)

$$1F_{fT} = \left(\frac{\sigma_{11}}{X_{1T}}\right)^2 + \alpha\left(\frac{\tau_{12}}{S_{12}}\right)^2 = 1 \tag{1}$$

Fiber Compression: ($\sigma_{11} < 0$)

$$F_{fC} = \left(\frac{\sigma_{11}}{X_{1C}}\right)^2 = 1 \tag{2}$$

Matrix Tension: ($\sigma_{22} \geq 0$)

$$F_{mT} = \left(\frac{\sigma_{22}}{X_{2T}}\right)^2 + \left(\frac{\tau_{12}}{S_{12}}\right)^2 = 1 \tag{3}$$

Matrix Compression: ($\sigma_{22} < 0$)

$$F_{mc} = \left(\frac{\sigma_{22}}{2S_{13}}\right)^2 + \left(\left(\frac{X_{2C}}{2S_{13}}\right)^2 - 1\right)\left(\frac{\sigma_{22}}{X_{2C}}\right) + \left(\frac{\tau_{12}}{S_{12}}\right)^2 = 1 \tag{4}$$

where σ_{11},σ_{22}, and τ_{12} are the components of the equivalent stress tensor. X_{1T}, X_{1C}, X_{2T}, X_{2C}, S_{12} and S_{13} refer to the longitudinal tensile, longitudinal compressive, transverse tensile, transverse compressive, longitudinal shear and transverse shear strengths respectively - see Table 3 for values. In this model, Hashin 2-D failure initiation criterion is adopted, where the fiber tensile is assumed to be independent from shear stress so alpha is assumed to be zero and $X_{2C} = 2S_{13}$.

4.3. Laminates' damage evolution

When Hashin's initiation criterion is satisfied for any failure load, any extending loading will lead to degradation of the material stiffness, and the general form of the constitutive law is computed as:

$$\sigma = C_d\varepsilon \tag{5}$$

where the stress and strain tensors are defined as $\{\sigma_{11},\sigma_{22},\sigma_{12}\}$ and $\{\varepsilon_{11},\varepsilon_{22},\varepsilon_{12}\}$ respectively, and the elasticity matrix (C_d) is given as:

$$C_d = \frac{1}{D}\begin{bmatrix} (1-d_f)E_{11} & (1-d_f)(1-d_m)\nu_{21}E_{11} & 0 \\ (1-d_f)(1-d_m)\nu_{21}E_{22} & (1-d_m)E_{22} & 0 \\ 0 & 0 & (1-d_s)G_{12}D \end{bmatrix} \tag{6}$$

where,

$$D = 1 - (1-d_f)(1-d_m)\,\nu_{12}\nu_{21} \tag{7}$$

d_f, d_m, and d_s are the current damage states of the fiber, matrix, and shear, respectively. They are derived from the four damage variables (d_f^t, d_f^c,d_m^t,d_m^c) as shown in equations (8,9,10) which are related to the four failure modes.

$$d_f = \begin{cases} d_f^c, \sigma_{11} < 0 \\ d_f^t, \sigma_{11} \geq 0 \end{cases} \tag{8}$$

$$d_m = \begin{cases} d_m^c, \sigma_{22} < 0 \\ d_m^t, \sigma_{22} \geq 0 \end{cases} \tag{9}$$

$$d_s = 1 - \left(1-d_f^t\right)\left(1-d_f^c\right)\left(1-d_m^t\right)\left(1-d_m^c\right) \tag{10}$$

The evolution of the damage variables of the four failure modes, fiber tension, fiber compression, matrix tension, and matrix compression, depends on the critical energy release rates, G_{IC}, in these modes, which are material properties. Therefore, critical energy release rate value must be provided for each mode which reflects the area of the triangle OAC illustrated in Figure 4. [15]

The constitutive laws are:

Tension: ($\sigma_{11} \geq 0$):

$$\delta_{eq}^{fT} = L_c\sqrt{\langle\varepsilon_{11}\rangle^2 + \alpha\varepsilon_{12}^2} \tag{11}$$

$$\sigma_{eq}^{fT} = \frac{\langle\sigma_{11}\rangle\langle\varepsilon_{11}\rangle + \alpha\sigma_{12}\varepsilon_{12}}{\delta_{eq}^{fT}/L_c} \tag{12}$$

Fiber Compression:($\sigma_{11} < 0$):

$$\delta_{eq}^{fC} = L_c\langle-\varepsilon_{11}\rangle \tag{13}$$

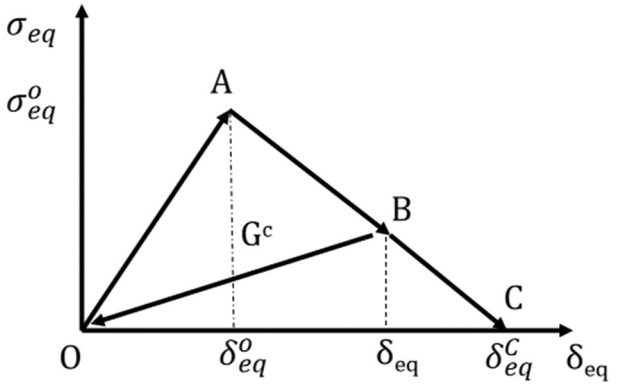

Figure 4. Equivalent stress vs equivalent displacement.

$$\sigma_{eq}^{f\,C} = \frac{\langle -\sigma_{11}\rangle\langle -\varepsilon_{11}\rangle}{\delta_{eq}^{f\,C}/L_c} \tag{14}$$

Matrix Tension:($\sigma_{22} \geq 0$):

$$\delta_{eq}^{mT} = L_c\sqrt{\langle \varepsilon_{11}\rangle^2 + \varepsilon_{12}^2} \tag{15}$$

$$\sigma_{eq}^{mT} = \frac{\langle \sigma_{22}\rangle\langle \varepsilon_{22}\rangle + \sigma_{12}\varepsilon_{12}}{\delta_{eq}^{mT}/L_c} \tag{16}$$

Matrix compression:($\sigma_{22} < 0$)

$$\delta_{eq}^{mC} = L_c\sqrt{\langle -\varepsilon_{22}\rangle^2 + \varepsilon_{12}^2} \tag{17}$$

$$\sigma_{eq}^{mC} = \frac{\langle -\sigma_{22}\rangle\langle -\varepsilon_{22}\rangle + \sigma_{12}\varepsilon_{12}}{\delta_{eq}^{mc}/L_c} \tag{18}$$

where δ_{eq} and $\sigma_{eq}$are the equivalent displacement and stress for each of the four damage modes,σ_{11}, σ_{22} andσ_{22} are the components of the effective stress tensor,ε_{11}, ε_{22} and ε_{12} are the components of the effective strain tensor and L_C is the characteristic length of the element to alleviate the mesh dependency during material softening. Since the plies in this simulation are modelled as a shell of elements, the characteristic length is calculated by taking the square root of the element surface area. In addition, $\langle\rangle$ refers to the Macaulay operator,[15] and defined as:

$\langle\eta\rangle = \frac{1}{2}(\eta + |\eta|)$, for every $\eta \in \Re$

For each failure mode, the degradation of the stiffness is being controlled by the damage variables, whose values varies between zero which represent the undamaged state and unity which refers to the fully damaged state. The damage variable for a particular mode is derived as:

$$d = \frac{\delta_{eq}^{f}\left(\delta\mathrm{eq} - \delta_{eq}^{0}\right)}{\delta\mathrm{eq}\left(\delta_{eq}^{f} - \delta_{eq}^{0}\right)} \tag{19}$$

The matrix fracture energy, G_{mc} for tension and compression are taken as the G_{Ic} value of carbon/epoxy composite, which is approximately 0.9 N/mm. This assumption is based on the fact that mode I delamination is mainly dominated by matrix cracking.[16] Tensile and compressive fiber fracture energy release rates could be obtained from compact tension (CT) and compression (CC) tests as proposed by Pinho et al.[17] The average critical energy release rate obtained by the experimental tests for carbon fiber tension is 133 N/mm with a standard deviation value of 15.7%. Also, the average critical energy release rate for fiber compression is 143 N/mm with a standard deviation of 10.5%. These values are summarized in Table 4.

4.4. Viscous regularization

Severe convergence difficulties in simulation's software, such as ABAQUS Standard may occur because of the stiffness degradation softening behavior of the material. The viscous regularization scheme helps overcoming such convergence difficulties since it makes the tangent stiffness matrix positive for relatively small increments of time.[15] The four viscous damage variables are derived by the following equations:

$$d_{ft}^{v} = \frac{1}{\eta_{fT}}\left(d_{ft} - d_{ft}^{v}\right) \tag{20 - a}$$

$$d_{fC}^{v} = \frac{1}{\eta_{fC}}\left(d_{fC} - d_{fC}^{v}\right) \tag{20 - b}$$

$$d_{mt}^{v} = \frac{1}{\eta_{mT}}\left(d_{mt} - d_{mt}^{v}\right) \tag{21 - a}$$

$$d_{mC}^{v} = \frac{1}{\eta_{mC}}\left(d_{mC} - d_{mC}^{v}\right) \tag{21 - b}$$

where, η is the viscosity coefficient for the specified failure mode that reflects the relaxation time of the system and d reflects the damage variable evaluated in the previous increment. Using viscous regularization with small values of

viscosity relative to the characteristic time increment is intended to improve the model convergence rate during the damage propagation. Viscous regularization is used so that the solution of the viscous system approaches the inviscid case at t/η→∞, where, *t* represents time.[15] Also, to help overcoming convergence difficulties, viscosity coefficients equal to10^{-4} in all damage modes are assumed as recommended by Hyder[18] in order to overcome convergence difficulties as well as having a simulation approximately accurate solution.

4.5. Tsai-Wu damage initiation criterion

Based on the experimental observation as detailed later in Section 5.2, the damage did not initiate from the adhesive joint. Moreover, a repair with a failure initiation in the adhesive is unacceptable for industrial applications.[19] Hence, the failure index computed from Tsai-Wu in the composite plies is assumed to represent the critical parameter at certain applied load. Tsai-Wu failure initiation criterion is adopted because the damage variable represents the interaction between different stress components. The failure criterion requires that:

$$I_f = \mathrm{F}_1\ \sigma_{11} + \mathrm{F}_2\ \sigma_{22} + \mathrm{F}_{11}\ \sigma_{11}^2 + \mathrm{F}_{22}\ \sigma_{22}^2 + \mathrm{F}_{66}\ \sigma_{12}^2 + 2\mathrm{F}_{12}\ \sigma_{11}\sigma_{22} = 1 \quad (22)$$

where:

$$\mathrm{F}_1 = \frac{1}{\mathrm{X_T}} + \frac{1}{\mathrm{X_C}} \quad (23-\mathrm{a})$$

$$\mathrm{F}_2 = \frac{1}{\mathrm{Y_T}} + \frac{1}{\mathrm{Y_C}} \quad (23-\mathrm{b})$$

$$\mathrm{F}_{11} = -\frac{1}{\mathrm{X_T}\ \mathrm{X_C}} \quad (24-\mathrm{a})$$

$$\mathrm{F}_{22} = -\frac{1}{\mathrm{Y_T}\ \mathrm{Y_C}} \quad (24-\mathrm{b})$$

$$\mathrm{F}_{66} = \frac{1}{\mathrm{S}_{12}^2} \quad (25-\mathrm{a})$$

$$\mathrm{F}_{12} = f\sqrt{\mathrm{F}_{11}\ \mathrm{F}_{22}} \quad (25-\mathrm{b})$$

where −1 < f < 1. The f value is assumed to be zero due to the ignorance of the biaxial stress at failure, and at $\mathrm{I_f} \geq 1$, damage will initiate.

Tsai-Wu failure theory, as in Equation 22, defines a 3D failure surface surrounding the origin where failure occurs if a state of stress is on or outside the surface using $\{\sigma_{11},\sigma_{22},\sigma_{12}\}$. However, if the stress state is inside the failure surface, I_f <1, then it does not provide much information. Thus, a parameter defined as the strength ratio/safety factor R is considered as the scaling factor, which represents how far the current stress state is from the failure surface. In other words, it is defined as the value that if multiplied by all the stress components $\{R*\sigma_{11},R*\sigma_{22},R*\sigma_{12}\}$, leads to $I_f = 1$. Moreover, the failure index ($\frac{1}{R}$), ranging from 0 to 1, is defined as the inverse of the safety factor (R).

5. Results and discussion

5.1. Intact laminates flexural properties and notch sensitivity

The load vs displacement curves, for the intact and notched laminates, obtained through the solver of ABAQUS Standard are compared to the experimental curves in Figure 5a and 5b. It can be noticed from Figure 5 that there is a good agreement of the elastic segments of the experimental and numerical curves in the intact and notched laminates. Moreover, the prediction of the ultimate load and flexural modulus of the intact and notched laminates is relatively good. However, in the case of the intact simulation, a noise at the end of the numerical curve is observed. This might be due to convergence issue due to localization in the last two increments during the simulation. It is logical that this only occurred in the intact specimen case as there is no specific location or stress concentration to guide the convergence or in other words for the damage to initiate and grow from a computational point of view. Moreover, as previously highlighted in section 4.1, The damage in the patch and parent laminate was based on 2D Hashin criterion in Abaqus which simulates four damage modes namely: fiber tension, fiber compression, matrix

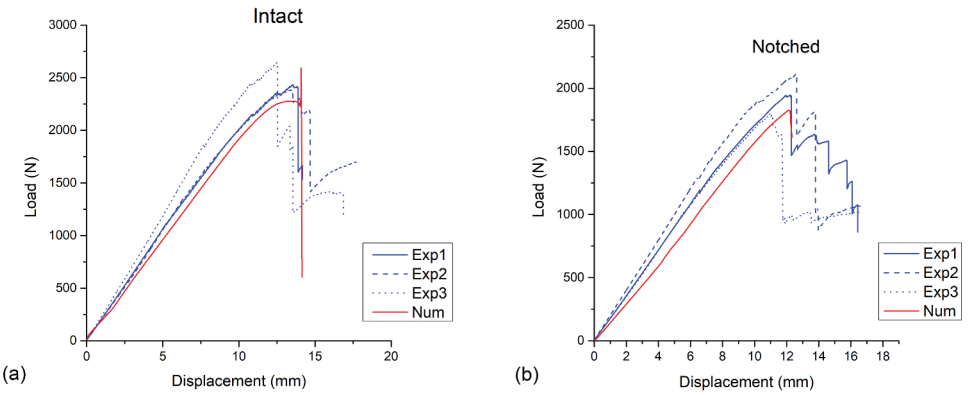

Figure 5. Numerical and experimental load vs displacement curves for: a) Intact specimen b) notched specimen.

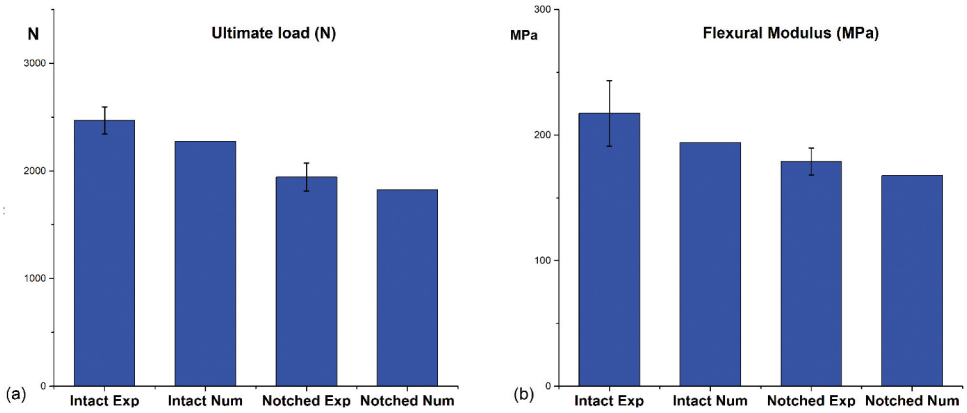

Figure 6. Intact and notched specimens' flexural properties: a) Ultimate load, b) Flexural modulus.

tension and matrix compression. No delamination or fiber pull out/debonding was simulated. The damage for these two cases occurred below the loading roller spanning across the specimens' width leading to such sudden drop in the load prediction without capturing the gradual crack growth observed experimentally. Figure 6a and Figure 6b show the average experimental flexural modulus and ultimate load values of the notched and intact laminates for the parent laminate $[0/90]_{3s}$. The notched laminate's ultimate load and flexural modulus are 0.823 and 0.787 normalized over the intact laminate values, respectively. It can be noticed from the flexural properties of the notched specimen for this specific hole diameter to width ration of 1/5 that the parent laminate close to notch insensitive response.[20] However, losing roughly 20% of the flexural properties is a significant value need to be restored by repairing.

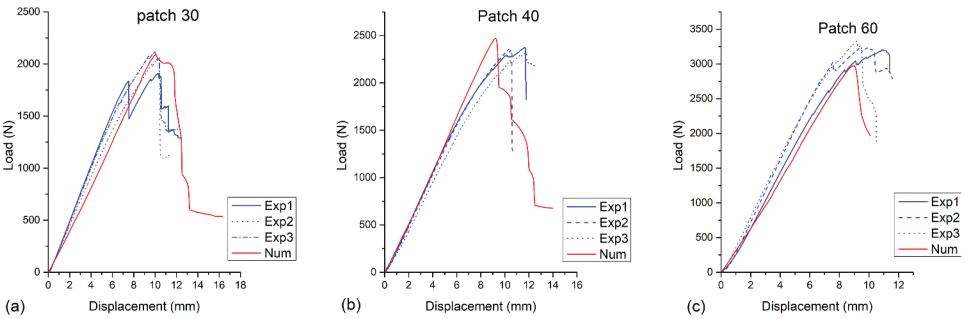

Figure 7. Numerical and experimental load vs displacement curves for: a) patch 30, b) patch 40, c) patch 60.

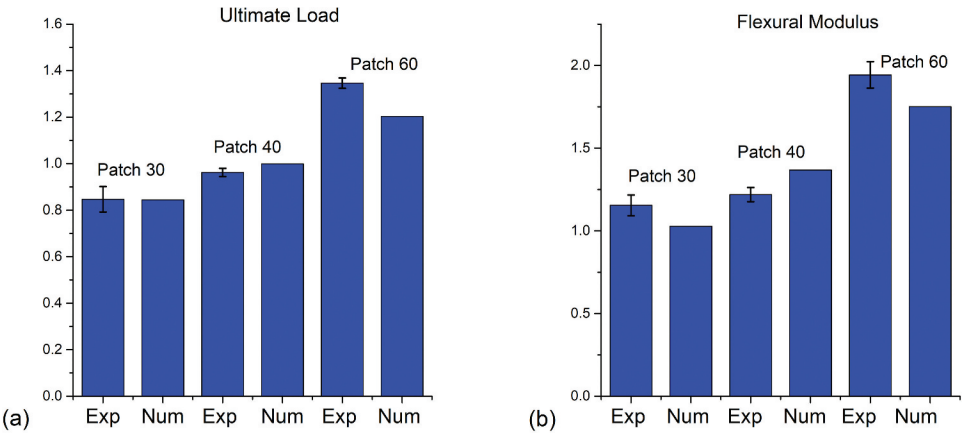

Figure 8. Intact, notched and patch-repaired specimens' flexural properties normalized over the intact laminates values: a) Ultimate load, b) Flexural modulus.

5.2. Effect of patch size on flexural modulus and ultimate load

From a failure investigation point of view, all samples, regardless of their patch size, failed due to interlaminar failure within the composite patch or parent laminate. No failure at the adhesive bondline was observed. As far as the macroscopic response is concerned, Figure 7a – 7c show the predicted load vs displacement curves for the repaired laminates of the $[0/90]_{3s}$ parent laminate, compared with the experimental curves. It can be noticed from Figure 7 that there is a fair prediction of the flexural modulus because the elastic segments of the numerical curves are within the experimental ones. Moreover, the prediction of the ultimate load of the repaired laminates is relatively good compared to the experimental values. From a macroscopic load–displacement point of view, the numerical predictions could not fully capture the sudden failure and the multiple-step crack growth. Nevertheless, this is expected as the model assumptions used are simplified with the objective of carrying out a parametric study (see Section 5.4) varying the patch size while maintaining the same failure modes. This can be considered a logical assumption since the testing is performed for the 30, 40, 60 sizes, and the numerical parametric study is within those limits (interpolation). Figure 8a and Figure 8b show the average experimental flexural modulus and ultimate values of the intact, notched and repaired laminates normalized over the intact laminates' values. It can be concluded that the flexural modulus and ultimate increase significantly with the patch size. The flexural modulus for the repaired laminates with patch-60 is 1.983 times the intact laminate value; however, for the patch-30 and patch-40, the flexural modulus is 1.145 and 1.215, respectively. The ultimate load of

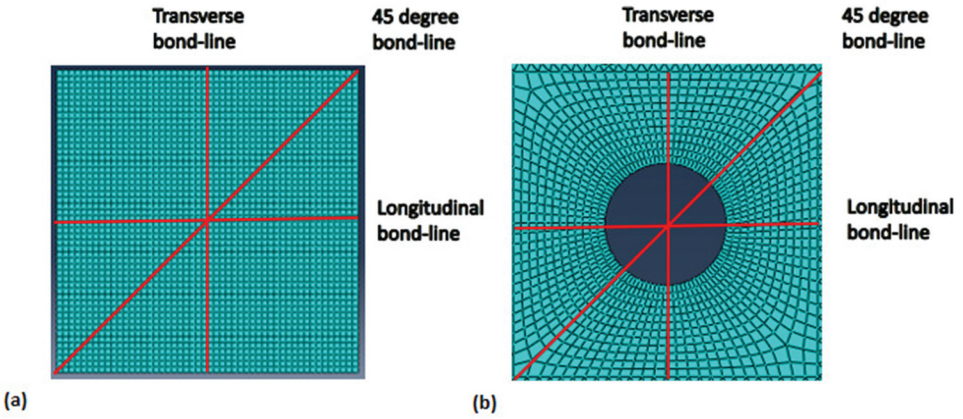

Figure 9. Longitudinal, transverse and 45 degree bond-lines: a) patch, b) parent laminate.

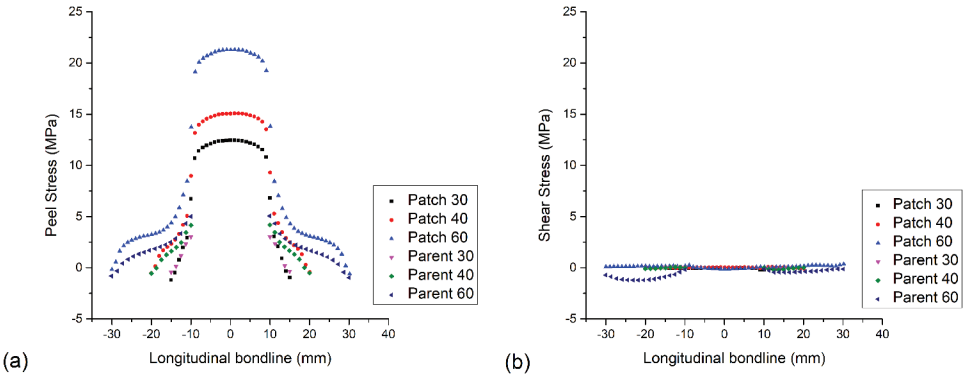

Figure 10. Stress distribution on the longitudinal bond–line interface of parent and patch laminates: a) peel stress, b) shear stress.

the repaired laminates with patch sizes of 30, 40, 60 is found to be 0.847, 0.962,1.346 times the intact laminate , respectively, as shown in Figure 8a and Figure 8b.

5.3. Peel and shear stresses along the bond-line

Peel and shear stresses along the bond-line are two of the main aspects influencing composite repair patch's failure.[4] For the sake of comparison, peel and shear stresses distribution on the patch and the parent laminate longitudinal, transverse and 45 degree bond-lines interface, as shown in Figure 9a,b, (composite and patch) are plotted in the elastic region, at 4 mm displacement as shown in Figure 10a, b, 11a, b and 12a, b. Peel and shear stresses on the patch are found to be higher than the parent laminate in all bond-lines. Peel stresses distribution are roughly the same in the longitudinal, transverse and 45 degree bond-line with a peak at the patch overlap with notch

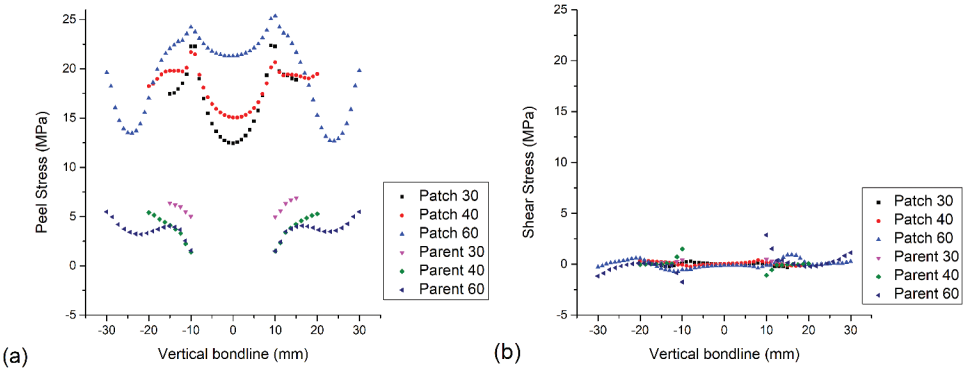

Figure 11. Stress distribution on the transverse bond–line interface of parent and patch laminates: a) peel stress, b) shear stress.

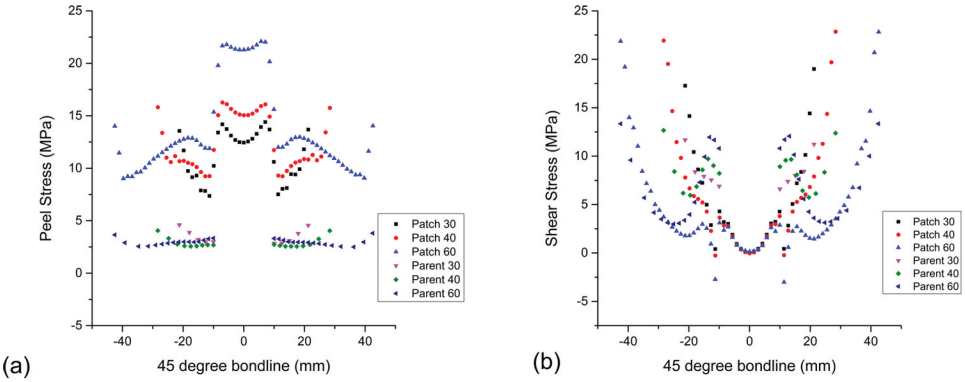

Figure 12. Stress distribution on the 45 degree bond–line interface of parent and patch laminates: a) peel stress, b) shear stress.

edge on the patch interface while the peak on the parent laminate interface is found to be at the patch edge overlap as shown in Figure 10a, 11a and 12a. On the other hand, shear stresses on the longitudinal and transverse directions are almost negligible but there are relatively high shear stresses on the 45 degree bond-line where the patch overlaps with parent laminate and the notch and patch corners as illustrated in Figure 10b, 11b and 12b. Peel stresses on patches are found to be increasing with the patch size along the three bond-lines. On the other hand, peel stresses on the parent laminate are roughly the same along the bond-lines.

5.4. Recommended patch size

A parametric study has been conducted for different patches' sizes from 30 to 60. As the objective of this study is to investigate the effectiveness of the patch repairs as compared to the notched case, the applied load at which damage

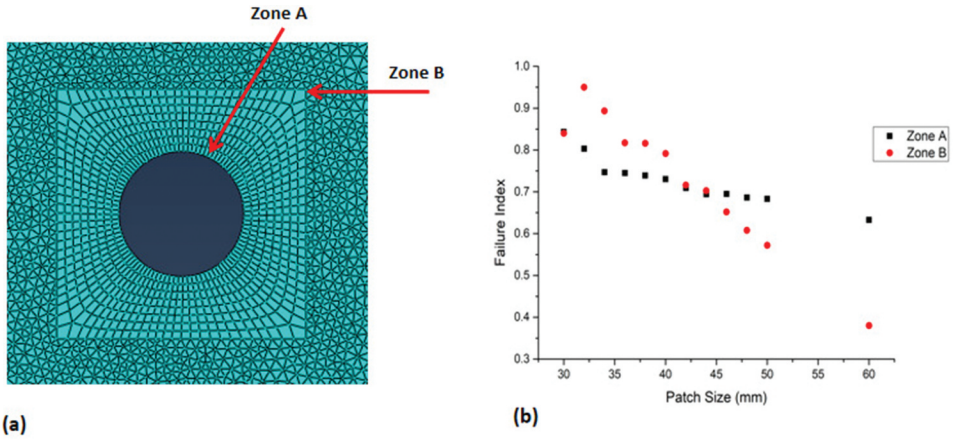

Figure 13. Critical zones and its failure initiation coefficient: a) Critical zones, b). Failure initiation coefficient.

initiates in the notch case is used for the comparison. The failure index ($\frac{1}{R}$) is plotted, as a function of the patch size, in order to determine the enhancement due to the repair. The factor of safety of different patch sizes at the applied load is represented as 1/the failure index.[19] Throughout the numerical modelling, the damage initiation always starts on the parent laminate's top and bottom plies. Hence, critical zones are highlighted as illustrated in Figure 13a, as: (Zone A) on the bottom ply at 67.5 degrees and (Zone B) on the top ply at the patch corner overlap on the parent laminate. According to the parametric study, the damage initiates from the patch corner overlap on the top ply of the parent laminate for patch sizes less than 44 mm as shown in Figure 13b. For larger patches, the damage initiates from zone A on the bottom ply of the parent laminate. To avoid the discontinuity at the sharp edge of the one-sided square patches, it is recommended to use patches larger than 44 mm, or with an area of 6.165 normalized over the notch's area. Moreover, the square patch of the size 44*44 mm ultimate load and flexural modulus are 1.047 and 1.435 normalized over the intact laminate values. In other words, the repaired laminate managed to restore the intact laminate flexural properties.

6. Concluding remarks

The influence of one-sided cross-ply square patch's size on the notched parent laminate was investigated in the light of the load vs displacement curves, flexural modulus and ultimate load, peel and shear stresses along the bond-line as well as damage initiation at the critical zones. The load vs displacement curves, flexural modulus and ultimate prediction, obtained through the progressive damage analysis via ABAQUS standard were within the deviation of the experimental values, indicating a good agreement of the used models.

Square one-sided patches were found to be beneficial for increasing the flexural modulus and ultimate load for the repaired specimen as compared to both notched and intact counterparts. Ultimate loads of the square patches with the sizes of 30*30 mm, 40*40 mm and 60*60 mm are 0.847, 0.962 and 1.346 while the flexural moduli are 1.154, 1.219 and 1.943 normalized over the intact laminate values. Shear stresses were observed only on the 45 degree bond-line with two peaks on the patch overlaps with the parent laminate's notch and patch corners. Peel stresses distribution were approximately the same in all the three bond-lines/patch sizes with a peak at the patch overlap with the notch edge. Based on the simulation results, the damage initiated on the top ply of the parent laminate at the patch corner overlap for patch's size less than 44*44 mm. Thus, it was concluded that the recommended patch's size of 44*44 mm or lager for a 20 mm notch as it led the edge discontinuity influence to disappear.

Disclosure statement

No potential conflict of interest was reported by the author(s).

ORCID

Mohamed Nasr Saleh http://orcid.org/0000-0002-0725-5319
Sofia Teixeira De Freitas http://orcid.org/0000-0002-0847-6287

References

[1] Zweben, C.;. Advanced Composites for Aerospace Applications: A Review of Current Status and Future Prospects. *Composites*. 0010-4361. 1981, *12*(4), 235–240. DOI: 10.1016/0010-4361(81)90011-2.
[2] Davies, P.;. Environmental Degradation of Composites for Marine Structures: New Materials and New applications.Phil. *Trans. R. Soc. A* 2016, *374*, 20150272. DOI: 10.1098/rsta.2015.0272.
[3] Baker, A.; Rose, L. R. F.; Jones, R. *Advances in the Bonded Composite Repair of Metallic Aircraft structure.*; Australia: Elsevier Science Ltd., 2002; pp 9.
[4] Mohammadi, S.; Yousefi, M.; Khazaei, M. A Review on Composite Patch Repairs and the Most Important Parameters Affecting Its Efficiency and Durability. *J. Reinf. Plast. Compos.* 2021, *40*(1–2), 3–15. DOI: 10.1177/0731684420941602.
[5] Budhe, S.; Banea, M. D.; de Barros, S. Bonded Repair of Composite Structures in Aerospace Application: A Review on Environmental Issues. *Appl. Adhes. Sci.* 2018, *6* (1). DOI: 10.1186/s40563-018-0104-5.
[6] Albedah, A.; Bachir Bouiadjra, B.; Mhamdia, R.; Benyahia, F.; Es-Saheb, M. Comparison between Double and Single Sided Bonded Composite Repair with Circular Shape. *Mater. Des.* 0261-3069. 2011, *32*(2), 996–1000. DOI: 10.1016/j.matdes.2010.08.022.

[7] Hu, F. Z.; Soutis, C. Strength Prediction of Patch-repaired CFRP Laminates Loaded in Compression. *Compos. Sci. Technol.* 0266-3538. 2000, *60*(7), 1103–1114. DOI: 10.1016/S0266-3538(00)00011-7.

[8] Campilho, R. D. S. G.; de Moura, M. F. S. F.; Ramantani, D. A.; Morais, J. J. L.; Domingues, J. J. M. S. Tensile Behaviour of Three-dimensional Carbon-epoxy Adhesively Bonded Single- and Double-strap Repairs. *Int. J. Adhes. Adhes.* 0143-7496. 2009, *29*(6), 678–686. DOI: 10.1016/j.ijadhadh.2009.02.004.

[9] Her, S.-C.; Chao, M. Adhesively Bonded Patch Repair of Composite Laminates. *J. Adhes. Sci. Technol.* 2011, *25*(18), 2569–2585. DOI: 10.1163/016942411X580234.

[10] Soutis, C.; Hu, F. Z. Design and Performance of Bonded Patch Repairs of Composite Structures. *Proc. Inst. Mech. Eng. Part G: J. Aerosp. Eng.* 1997, *211*(4), 263–271. DOI: 10.1243/0954410971532668.

[11] Li, K.; Ch Tie Y, L.; Yu, Y. Influence of Patch Parameters on Damage and Residual Strength of Adhesively Bonded Composite Repair under Fatigue Loading. *Mater. Phys. Mech.* 2015, *24*, 391–402.

[12] Xiao-Jing, G.; Cheng, P.; Rousseau, J.; Shahram, A. Effect of Local Stresses on Static Strength and Fatigue Life of Patched Composite Panels. In: 16th International conference on composite materials (ICCM-16) 2007. Kyoto, Japan 2007.

[13] Tsovolos, A.; Giannakopoulos, K. I.; Zhang, Z.; Tsamasphyros, G. I.; Kanderakis, G.; Kalkanis, K.; Vouthounis, P.; Katerelos, D.; Dhakal,; Dhakal, H. N. Hom. Composite Structure Repair Scheme Assessment. *Sensor Letters* 2015, *13*(5), 405–410. DOI: 10.1166/sl.2015.3469.

[14] Deng, J.; Zhou, G.; Kerfriden, P.; Bordas, S.; Yin, Q. Progressive Damage Analysis on Yielding of Bonded Patch Repaired Composite Laminates under Compressive Loading. 2016.

[15] Dassault Systemes, ABAQUS/CAE User's Guide, From ABAQUS 6.14 Online Documentation, (2014) http://ABAQUS.software.polimi.it/v6.14/books/usi/default.htm

[16] Jye Wong, K.;. Moisture Absorption Characteristics and Effects on Mechanical Behaviour of Carbon/epoxy Composite: Application to Bonded Patch Repairs of Composite Structures. , 2013. . (France: Universite de Bourgogne)

[17] Pinho, S. T.; Robinson, P.; Iannucci, L. Fracture Toughness of the Tensile and Compressive Fibre Failure Modes in Laminated Composites. *Compos. Sci. Technol.* 0266-3538. 2006, *66*(13), 2069–2079. DOI: 10.1016/j.compscitech.2005.12.023.

[18] Hyder, I.;. ; USA: Oregon State University, 2014 Evaluation of Abaqus for simulating quasi-static Mode III shear of edge notched carbon fiber reinforced polymer panels .

[19] Gong, X.-J.; Cheng, P.; Aivazzadeh, S.; Xiao, X. Design and Optimization of Bonded Patch Repairs of Laminated Composite Structures. *Compos. Struct.* 2015, *123*, 292–300. 0263-8223. DOI: 10.1016/j.compstruct.2014.12.048.

[20] Saleh, N.; Mohamed,; Wang, Y.; Yudhanto, A.; Joesbury, A.; Potluri, P.; Lubineau, G.; Soutis, C. Investigating the Potential of Using Off-Axis 3D Woven Composites in Composite Joints' Applications. *Appl. Compos. Mater.* 2017, *24*, 1–20. DOI: 10.1007/s10443-016-9529-9.